6th European Conference on Computational Mechanics (ECCM 6)
7th European Conference on Computational Fluid Dynamics (ECFD 7)
11–15 June 2018, Glasgow, UK

USING ISOGEOMETRIC ANALYSIS OF TURBULENT FLOWS ON MOVING DOMAINS TO ASSESS THE FLUTTER STABILITY LIMIT OF LONG-SPAN SUSPENSION BRIDGES

TORE A. HELGEDAGSRUD[1,*], YURI BAZILEVS[2], KJELL M. MATHISEN[1] AND OLE A. ØISETH[1]

[1] Dept. of Structural Engineering, Norwegian University of Science and Technology (NTNU)
Richard Birkelands v 1a, NO-7491 Trondheim, Norway
∗*Email address:* tore.a.helgedagsrud@ntnu.no

[2] School of Engineering, Brown University,
184 Hope Street, Providence, RI 02912, USA

Key words: *Isogeometric Analysis, Bluff Body Aerodynamics, Bridge Engineering, Aerodynamic Derivatives, Wind Tunnel Experiments*

Abstract. We investigate using Isogeometric Analysis (IGA) of turbulent flows of moving domains to assess the flutter stability limit of long-span bridges by the forced-vibration method. In order to verify the simulations, we compare the results directly to the corresponding forced-vibration wind tunnel experiments. In addition, the derived flutter characteristics are compared to free-vibration wind tunnel experiments. The numerically and experimentally obtained aerodynamic derivatives are in very good agreement, and in terms of the flutter mode shape and critical wind speed, the simulations produce equally good estimates as the experiments. The present work proves IGA to be a reliable tool in engineering design and analysis of long-span bridge aerodynamics.

1 INTRODUCTION

Aeroelastic stability is one of the major concerns in the design of long-span suspension bridges, and recent developments in computational power and technology have made Computational Fluid Dynamics (CFD) and Fluid-Structure Interaction (FSI) important supplements to the conventional wind tunnel experiments.

In this work we employ Isogeometric Analysis (IGA) based on Non-Uniform Rational B-Splines (NURBS) to the Arbitrary Lagrangian-Eulerian Variational Multiscale (ALE-VMS) formulation for incompressible flows on moving domains [9] to perform numerical

simulation of the forced-vibration wind tunnel experiment. The bridge section considered is a 1:50 scale model of the Hardanger bridge [37], which is a representative for many generic bridge sections. In the forced-vibration method [34] the sectional model is driven in a user-defined motion, from which the motion-induced forces governing the aerodynamic derivatives are measured. As this method only leads a one-way fluid-structure coupling, and requires a relatively small simulation time window, the problem can be solved very effectively and is well suited for numerical simulations.

The aerodynamic derivatives are transfer functions between body motion and forces, and are therefore commonly regarded as aerodynamic damping and stiffness [30]. When the aerodynamic derivatives are included in the equations of motion, the properties of the dynamic system alters with the wind speed, and at some point, one mode may experience zero damping. This instability phenomenon is referred to as flutter, and must be carefully taken into account in the design of long-span bridges. The Norwegian Public Road Administration requires that all bridges with the lowest natural frequency < 0.5 Hz and span width > 300 m are investigated for this instability [35].

The present work focuses on the aerodynamic derivatives and their application in the study of the flutter stability limit. In order to verify the simulations, we perform comparative forced-vibration wind tunnel experiments. We then use the numerically and experimentally obtained results to predict the corresponding flutter characteristics. To check the validity of these predictions, free-vibration wind tunnel experiments of the same dynamic system are used to provide the actual flutter characteristics.

This paper is outlined as follows. We present the computational strategy in Sec. 2. In Sec. 3 the relevant theory of bridge aeroelasticity is presented. The setup for wind tunnel experiments and simulations are given in Secs. 4 and 5, respectively. The results are reported in Sec. 6 before conclusions are drawn in Sec. 7.

2 COMPUTATIONAL METHOD

This section gives a brief summary of the computational framework employed in this work. We do not present any discrete equations, so for a more comprehensive introduction the reader is referred to the given references.

2.1 Fluid mechanics

The fluid mechanics part of the problem is governed by the Navier–Stokes equations of incompressible flows. On a spatial fluid mechanics domain $\Omega_t \in \mathbb{R}^{n_{sd}}$, $n_{sd} = 2, 3$ with

boundary Γ_t, with subscript t indicating time-dependence, they can be written as

$$\rho \left(\left. \frac{\partial \mathbf{u}}{\partial t} \right|_{\hat{x}} + (\mathbf{u} - \hat{\mathbf{u}}) \cdot \nabla \mathbf{u} - \mathbf{f} \right) - \nabla \cdot \boldsymbol{\sigma} = 0, \tag{1}$$

$$\nabla \cdot \mathbf{u} = 0. \tag{2}$$

In Eqs. 1–2, ρ is the density, $\mathbf{f}$ is the body force, $\mathbf{u}$ is the fluid velocity and $\hat{\mathbf{u}}$ is the fluid-domain velocity. The latter arises from the ALE description [25], and handles the moving domain. The subscript $|_{\hat{x}}$ on the partial derivative denotes that the time-derivative is taken with the referential coordinates $\hat{\mathbf{x}}$ kept fixed. The spatial derivatives are taken with respect to the current coordinates $\mathbf{x}$. $\boldsymbol{\sigma}$ is the fluid Cauchy stress tensor, given by

$$\boldsymbol{\sigma}(\mathbf{u}, p) = -p\mathbf{I} + 2\mu\, \boldsymbol{\varepsilon}(\mathbf{u}), \tag{3}$$

where p and μ are the fluid pressure and dynamic viscosity, respectively, and $\boldsymbol{\varepsilon}(\mathbf{u})$ is the symmetric gradient of $\mathbf{u}$.

At the discrete level we take the variational formulation of Eqs. 1 and 2 and make use of the stabilized Residual-Based Variational Multiscale (RBVMS) method. The RBVMS method for incompressible flows was developed for steady problems in [23, 24, 26] and extended to moving-domains (referred to as ALE-VMS) in [4] and decomposes the solution spaces into coarse and fine scales. The latter contains the turbulent structures which are not resolved within the weighting and test functional spaces, and are approximated by means of the coarse-scale residuals and stabilization parameters. The stabilization is based on Streamline-Upwind/Petrov-Galerkin (SUPG) and Pressure-Stabilizing/Petrov-Galerkin (PSPG) formulations [10, 20, 22, 41, 45, 47, 48], and are designed to render optimal convergence with respect to the element size and polynomial order of the discretization.

The formulation is augmented with weak enforcement of the essential boundary conditions [6–8, 18]. This method relaxes the no-slip boundary condition by replacing them with tractions that are driven in a penalty-like fashion by the deviation from the prescribed solution. The flow is then allowed to slip on solid boundaries and the classical restrictions on boundary-layer mesh size is alleviated. This leads to more accurate results on meshes that are too coarse to resolve the boundary-layers. In mesh refinement the formulation converges towards the strongly-enforced boundary conditions. Although purely numerics-based, the formulation was shown in [6] to behave as a near-wall function.

The ALE-VMS formulation with weakly-enforced boundary conditions has proven very powerful through a wide range of engineering problems, see e.g., [1–3, 5, 9, 15, 17, 38, 39, 41].

2.2 Mesh motion

From the domain-velocity $\hat{\mathbf{u}}$, introduced in conjunction with the ALE formulation in Sec. 2.1, we are able to "track" surfaces that are moving in the fluid domain. Hence, we refer to ALE as an interface-tracking method [45]. To accommodate the fluid mesh to the surface motion, we employ an automatic mesh-moving scheme where the fluid interior nodes are displaced by solving the equations of elasticity. This technique was introduced in [28, 44, 46] and further developed in [36]. Incorporated from the latter, we make use the Jacobian-based stiffening, in which the Young's modulus is assigned based on the element size. Small elements become stiffer and mesh distortion is kept to a minimum. This is clearly illustrated in Fig. 1, which shows different configurations of a test mesh

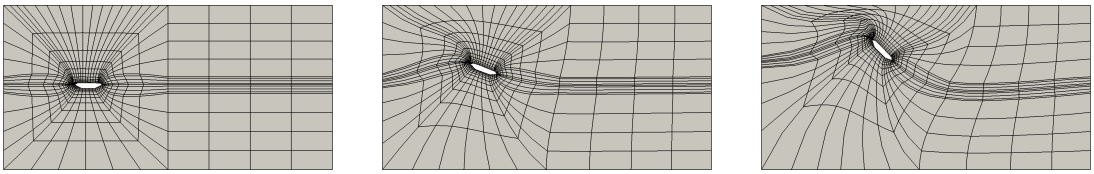

Figure 1: Fluid mesh deformation states computed on a coarse mesh undergoing large deformations.

undergoing relatively large deformations. Note how the region of small elements appear nearly undeformed.

2.3 Forced-vibration formulation for a rigid object

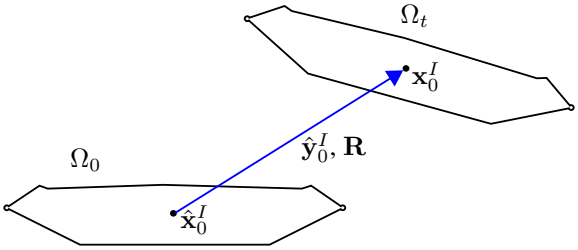

Figure 2: Rigid body in its reference and current configuration.

Given an object embedded in the fluid domain, we let $\hat{\mathbf{x}}^I$ and $\hat{\mathbf{x}}_0^I$ denote the reference coordinates of its fluid-object interface and centroid, respectively. Any rigid-body displacement can then be expressed in terms of a displacement and a rotation of the centroid. In terms of a user-defined displacement vector $\hat{\mathbf{y}}_0^I(t)$ and rotation matrix $\mathbf{R}(t)$, the position

of the fluid-object interface is given as

$$\hat{\mathbf{y}}^I(t) = (\mathbf{R}(t) - \mathbf{I})\left(\hat{\mathbf{x}}^I - \hat{\mathbf{x}}_0^I\right) + \hat{\mathbf{y}}_0^I(t). \tag{4}$$

In the interface-tracking technique, we use Eq. 4 to define the essential boundary conditions for the fluid mesh problem.

2.4 Time integration and equation solving

For time integration we use the Generalized-α method [5, 12, 27], and within each time step a predictor-multicorrector Newton-Raphson scheme is used. In a forced-vibration setting we get a one-way coupling between the fluid-mechanics and fluid mesh problem, which can be solved very effectively in a staggered fashion as described in [16].

2.5 Isogeometric analysis

For space discretization we employ NURBS-based IGA. In the concept of IGA was proposed in [21] and has been successfully employed to turbulent flows and VMS methods in many recent works, see e.g., [2, 4, 5, 8, 17, 19, 29, 40, 42, 43]. NURBS [32], which are the most popular basis function-technology in IGA, is used simultaneously for geometry modeling and interpolation spaces for analysis.

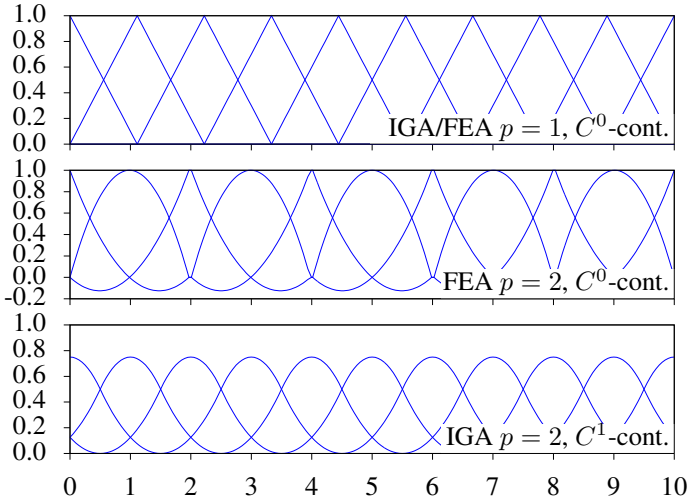

Figure 3: One-dimensional basis functions. Top: C^0-linear IGA and FEA. Center: C^0-quadratic FEA. Bottom: C^1-quadratic IGA.

Similar to Finite-Element Analysis (FEA), IGA uses a variational framework to discretize partial differential equation systems, and shares the attributes of the isoparametric

concept with h- and p-refinement. Unique for IGA are the options of including higher-order inter-element continuity and the so-called k-refinement, in which the polynomial order and smoothness of the basis functions are raised simultaneously. This refinement strategy is illustrated in Fig. 3, which compares the p-refined FEA and k-refined IGA interpolation functions. Thanks to the smooth solution spaces and the geometric flexibility of NURBS, IGA has proven to generally outperform FEA in terms of per-degree-of-freedom accuracy [4, 13].

Despite its excellent performance, IGA for volumetric meshes is much less developed than for shells and beams due to the lack of geometry modeling tools. Most volumes must therefore be constructed manually, which can be quite challenging and time-consuming.

3 BRIDGE AEROELASTICITY

In this section we give a brief introduction to bridge aerodynamics. We focus on the motion-induced part, which is one of the major concerns in long-span bridge design, however, other aspects as VIV and buffeting are also of great importance. For more details, the reader is referred to [11].

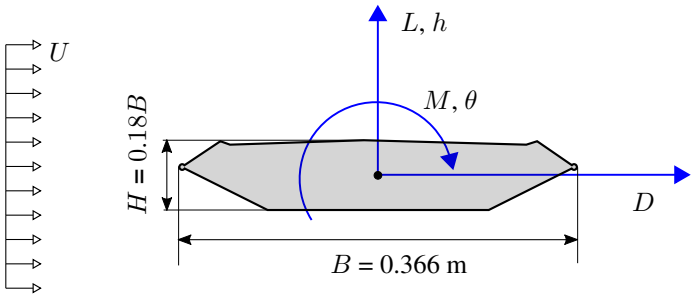

Figure 4: Rigid body in its reference and current configuration.

Following the notations and conventions in Fig. 4 we define the aerodynamic drag, lift and pitching moment acting on a unit chord length of a bridge deck centroid respectively as

$$D = \frac{1}{2}\rho U^2 H C_D(t), \tag{5}$$

$$L = \frac{1}{2}\rho U^2 B C_L(t), \tag{6}$$

$$M = \frac{1}{2}\rho U^2 B^2 C_M(t). \tag{7}$$

Here, U is the mean wind velocity, ρ is the air density, H and B are the height and the

width of the bridge deck, respectively, and $C_D(t)$, $C_L(t)$ and $C_M(t)$ are the instantaneous aerodynamic coefficients of drag, lift and pitching moment, respectively.

Disregarding the drag component, the self-excited part of the aerodynamic forces are commonly expressed on the semi-empirical form as proposed in [33]:

$$L^{se} = \frac{1}{2}\rho U^2 B\left(KH_1^*\frac{\dot{h}}{U} + KH_2^*\frac{B\dot{\theta}}{U} + K^2H_4^*\frac{h}{B} + K^2H_3^*\theta\right), \tag{8}$$

$$M^{se} = \frac{1}{2}\rho U^2 B^2\left(KA_1^*\frac{\dot{h}}{U} + KA_2^*\frac{B\dot{\theta}}{U} + K^2A_4^*\frac{h}{B} + K^2A_3^*\theta\right), \tag{9}$$

where h and θ are the heaving and pitching degrees-of-freedom, respectively, $K = B\omega/U$ is the reduced frequency of the structural motion, and H_i^* and A_i^*, $i \in \{1, ..., 4\}$ are the so-called flutter derivatives. These are commonly given as functions of the reduced velocity, $U_{red} = K^{-1}$. Superscript se denotes that its attribute is self-excited.

On matrix notation the self-excited forces read

$$\mathbf{q}^{se} = \mathbf{C}_{ae}\dot{\mathbf{r}} + \mathbf{K}_{ae}\mathbf{r}, \tag{10}$$

where $\mathbf{q}^{se} = [L^{se}, M^{se}]^T$, $\mathbf{r} = [h, \theta]^T$ and $\mathbf{C}_{ae}$ and $\mathbf{K}_{ae}$ contains the velocity- and position-dependent aerodynamic derivatives, respectively.

Including the self-excited forces in the equation of motion, we get a dynamic system which alters with the wind speed. Typically, a moderate wind speed adds a lot of damping, however, at some point the damping switches sign and the dynamic system exhibit an exponentially diverging response. This phenomena is knowns as flutter. The lowest wind speed at which flutter occur is known as the critical wind speed, U_{cr}, and is a crucial value in engineering design. The critical wind speed is calculated by determining the aerodynamic derivatives and thereafter solving the complex eigenvalue problem of the equations of motion. A detailed description is given in [31].

4 WIND TUNNEL EXPERIMENTS

For wind tunnel testing of bridge sectional models there are two strategies: forced-vibration and free-vibration. In the former the sectional model is driven in an user-defined motion, mostly harmonic, and the corresponding forces are measured. To determine the aerodynamic derivatives' variation with K, test are conducted at different wind speeds and/or vibration frequencies. In the free-vibration experiment, the sectional model is suspended in springs that typically scales the first heaving and pitching mode, and excited at different wind speeds. Displacement are estimated from the measured spring forces, from which the aerodynamic derivatives can be calculated. This method also has the advantage of being able to determine the model scale flutter speed directly.

Figure 5: The Hardanger bridge deck sectional model installed for forced-vibration (left), and free-vibration wind tunnel experiments (right).

The free-vibration experiment has a cheap and easy setup compared to the forced-vibrations. However, since the latter leads to a less scattered and a much easier identification procedure for the aerodynamic derivatives, this is often the preferred method for sectional model testing of bridge decks [14, 34].

In this work we use the forced-vibration method to determine the aerodynamic derivatives of the 1:50 scale model of the Hardanger bridge sectional model. A detailed description of the experimental setup and the identification procedures are given in [34]. The section is tested under harmonic motions from 0.5 to 2.5 Hz at wind speeds in the range of 4 to 12 m/s, see Tab.1. These results are reported in [15].

Additionally, free-vibration experiments of the very same sectional model are performed in order to validate the critical wind speed and the corresponding vibration mode. This experimental setup was designed to proportionally copy the full scale modal quantities of the Hardanger bridge [30] and is otherwise conducted as described in [37]. It should be remarked that the two experiments have been conducted under as similar conditions as possible.

The pictures in Fig. 5 shows the bridge deck section model installed in the forced- and free-vibration rig, respectively.

5 ANALYSIS SETUP

The computational domain is taken as a 0.25 m wide slice of the wind tunnel, whose total width is 2.7 m. The ceiling and floor are placed 0.930 and 0.885 m from the bridge deck centroid, respectively, matching the physical dimensions. These surfaces are enforced with no-penetration. The inflow surface, with a prescribed uniform wind velocity U, is placed 1.0 m upwind from the centroid, whereas the traction-free outflow surface

is placed 3.0 m downwind. The bridge deck surface is subjected to the weakly-enforced boundary conditions.

For the mesh-moving boundary conditions, the surface nodes of the bridge deck is enforced by Eq. 4. For the other surfaces, the nodes are not allowed to move out of plane, as also seen in Fig. 1.

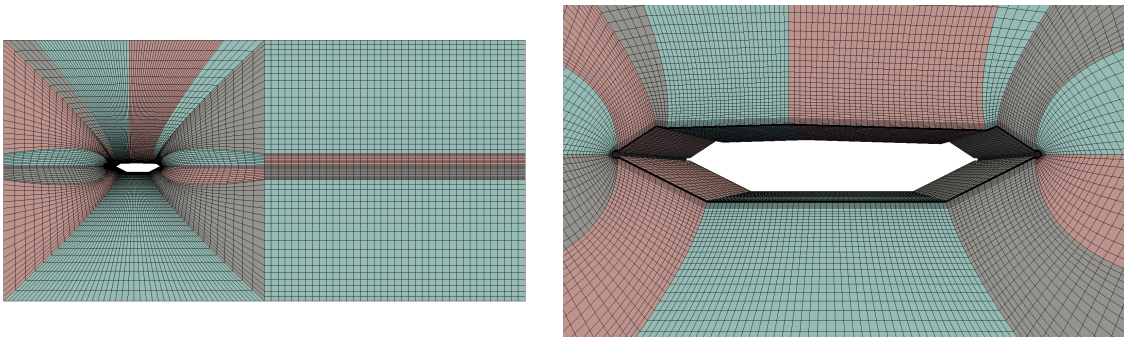

Figure 6: Patch topology and mesh density of the computational domain.

The 3D domain is constructed by 17 C^1-quadratic NURBS patches. An outline of the computational model is shown in Fig. 6, which shows the patch topology and the general mesh density. For visualization the NURBS elements are mapped onto linear hexahedrals. The nodes are clustered towards the bridge deck, with a thickness of the boundary layers that gives $y^+ \approx 6$. The total number of computational nodes, or control points, is 313×10^3 and the computations are performed in an parallel environment adopted from [17] on 256 subprocesses.

The air density is set to $\rho = 1.1835\ \mathrm{kg/m^3}$ and the dynamic viscosity to $\mu = 1.848 \times 10^{-5}\ \mathrm{kg/ms}$. The computational time-stepping is set to 7×10^{-5} s, giving a maximum CFL number below 5.

The test strategy for the forced-vibration simulations and experiments are summarized in Tab. 1. We see that the chosen frequencies and velocities render $U_{red} \in [2, 7]$, which are assumed to enclose the modes of interest, including flutter.

6 RESULTS AND DISCUSSION

6.1 Aerodynamic derivatives

Fig. 7 shows the numerically and experimentally obtained aerodynamic derivatives from the forced-vibrations. For a continuous representation, least-square fitted 3^{rd} order polynomials are drawn. Fig. 8 shows the flow field around the bridge deck at different pitching angles and emphasizes the turbulent nature of the problem, although the bridge section has a streamlined shape.

Table 1: Test strategy for the forced-vibration experiments and simulations.

	Simulations	Wind tunnel
Amplitude h	15 mm	15 mm
Amplitude θ	2°	2°
Wind velocities	8 m/s	4, 8, 10 and 12 m/s
Vibration frequencies	0.5, 0.8, 1.1 and 2.0 Hz	0.5, 0.8, 1.1, 1.4, 1.7, 2.0 and 2.5 Hz
Number of cycles	2	25 – 100
Sampling frequency	250 Hz	200 Hz

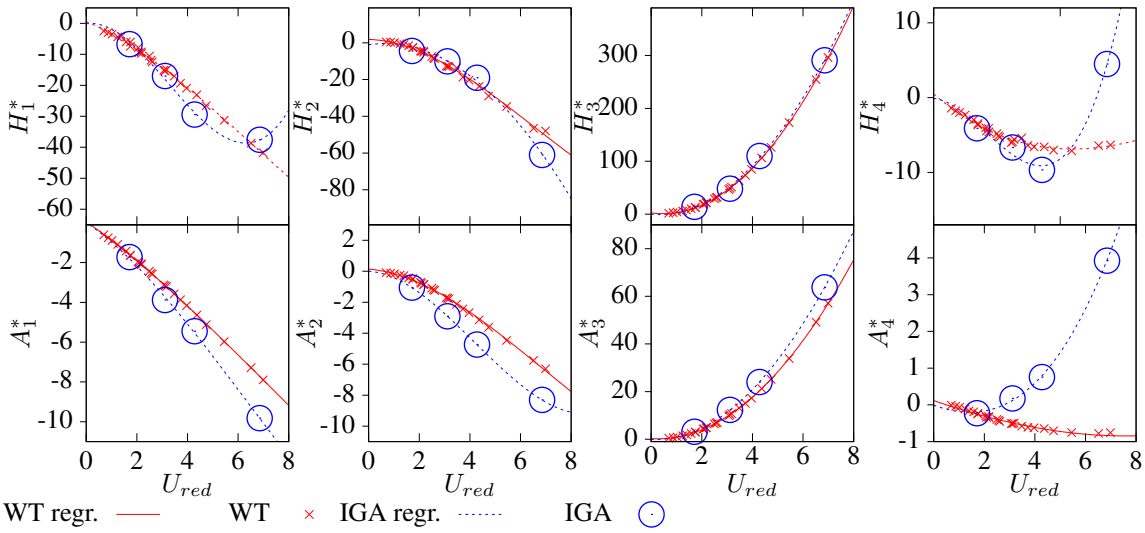

Figure 7: Aerodynamic derivatives obtained by forced-vibration wind tunnel experiments (WT) and numerical simulations (IGA).

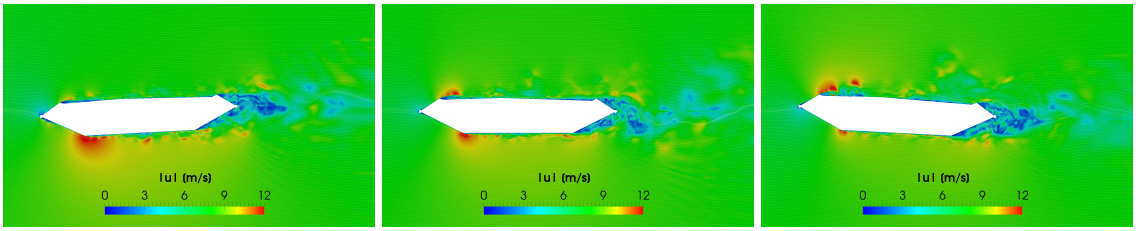

Figure 8: Instantaneous velocity contours for the IGA simulation undergoing the 0.5 Hz pitching motion. Left to right: $\theta = -2°, 0°$and 2°.

The closely matching aerodynamic derivatives prove that IGA captures the aeroelastic behavior of the bridge section with very good accuracy. It is remarked however, that the simulations generally render a slightly higher magnitude of the self-excited forces than the experiments.

6.2 Free-vibrations and flutter

Table 2: Still-air properties of the dynamic system tested in the free-vibration experiments. Full scale data [30] are shown for comparison.

		Experiment	Full scale	
Mass	m	5.12	12820	$\mathrm{kg/m}$
Inertia	$I_{\theta\theta}$	0.083	426 000	$\mathrm{kgm^2/m}$
Vertical natural frequency	ω_h	5.01	0.89	$\mathrm{rad/s}$
Torsional natural frequency	ω_θ	12.64	2.23	$\mathrm{rad/s}$
Mechanical damping vertically	ζ_h	3.8e-3	6.0e-3	$-$
Mechanical damping torsionally	ζ_θ	1.2e-3	5.0e-3	$-$

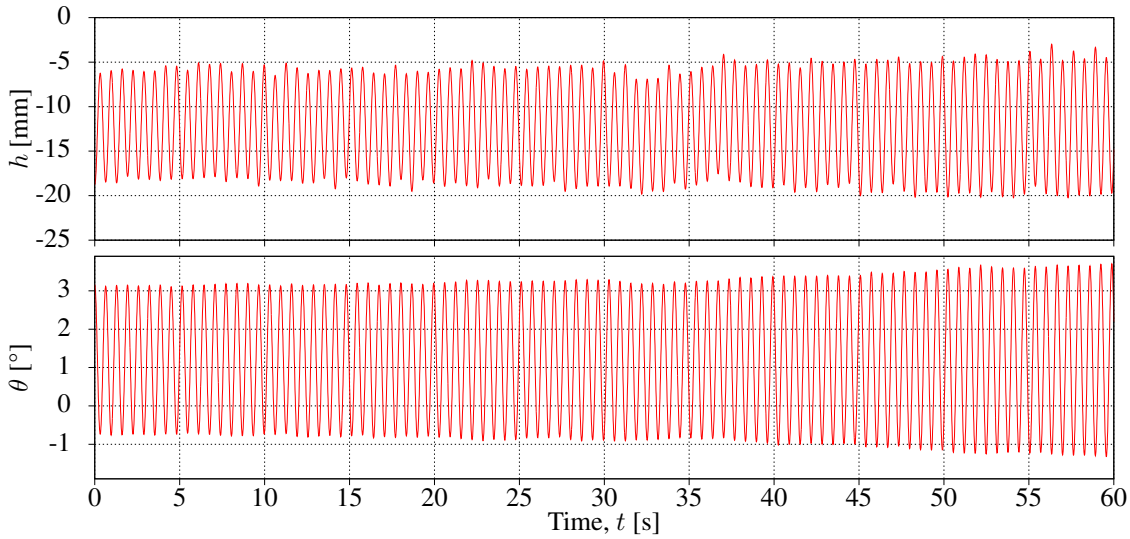

Figure 9: Time series for heaving and pitching from the free-vibration wind tunnel experiment at $U = U_{cr}$.

The still-air properties of the sectional model when installed for free-vibration experiments are summarized in Tab. 2. The comparative full scale quantities corresponds to the modal values of the first heaving and pitching mode and are taken from [30]. The critical

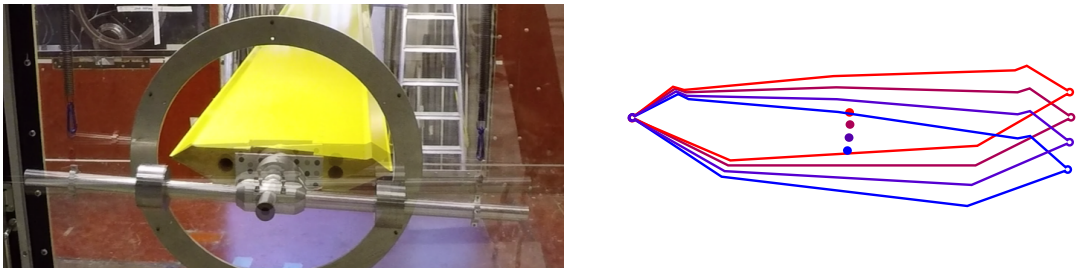

Figure 10: Visualization of the flutter mode. Overlay pictures from the experiment (left) and outlines of the cross-section (right).

flutter wind speed was determined to $U_{cr} = 8.16$ m/s with a corresponding vibration frequency of $\omega_{cr} = 9.80$ rad/s. The reader should however be aware that, for soft flutter, the experimentally determined value of U_{cr} is often associated with some uncertainty.

A one minute time window of the flutter experiment is shown in Fig. 9, revealing the stationary non-decaying response. Fig. 10 visualizes the flutter mode where the bridge section appears to rotate about its leading edge.

6.3 Predictions based on forced vibrations

Based on the computed aerodynamic derivatives from the IGA simulations, as well as the forced-vibration experiments from Sec. 6.1, we now solve the complex eigenvalue problem to predict the flutter characteristics that was experimentally determined in Sec. 6.2. Following from Sec. 3 the eigenvalue problem takes the form:

$$\mathbf{M}_0\ddot{\mathbf{r}} + (\mathbf{C}_0 - \mathbf{C}_{ae})\,\dot{\mathbf{r}} + (\mathbf{K}_0 - \mathbf{K}_{ae})\,\mathbf{r} = \mathbf{0}, \tag{11}$$

where subscript 0 refers to the still-air quantities. Since the aerodynamic derivatives depend on both the wind speed and the vibration frequency, Eq. 11 is solved iteratively. The resulting flutter characteristics are summarized in Tab. 3 and Figs. 11 and 12 compares the predicted flutter modes to the free-vibrations.

Table 3: Experimentally and numerically obtained flutter characteristics. φ refers to the phase lag between the pitching and heaving motion.

		Free-vibr. exp.	Forced-vibr. exp.	IGA	
Flutter wind speed	U_{cr}	8.16	7.49	7.99	m/s
Critical frequency	ω_{cr}	9.80	10.12	9.17	rad/s
Phase angle	φ	180.7	183.4	176.7	°

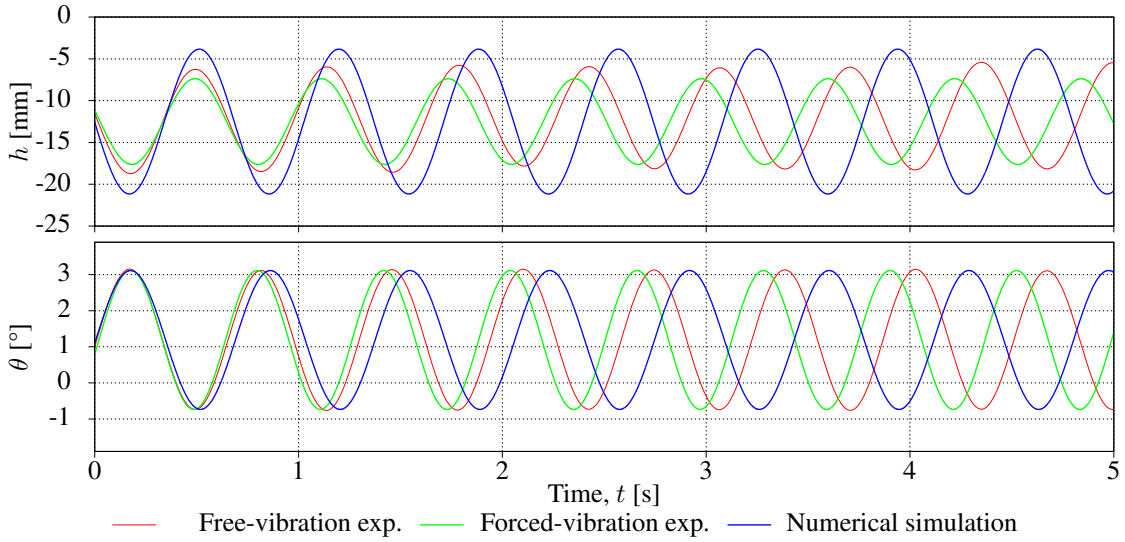

Figure 11: Forced-vibration predictions of the flutter mode based on experiments and simulations compared with the free-vibrations.

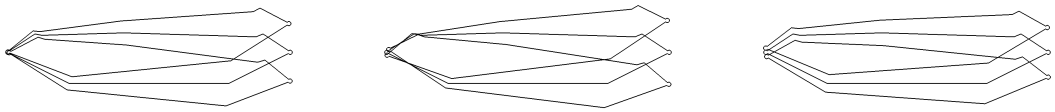

Figure 12: Flutter mode shapes. From left to right: Free- and forced-vibration wind tunnel experiment and forced-vibration numerical simulation.

Firstly, we notice that the forced-vibration method generally predicts the flutter characteristics with good accuracy, and while the experiments give a more accurate prediction of the mode shape, the simulations render a more correct value of the critical wind speed. The discrepancies between the free- and forced-vibration experiments emphasize that the results are associated with some uncertainties. This could obviously result from deviations and inaccuracies in the experimental setup, but also weaknesses or shortcomings of the load theory, which after all is based on numerous simplifications. Even so, the numerical simulations produce convincingly accurate results and prove the validity of the computational framework.

7 CONCLUSIONS

In this work we used NURBS-based IGA of the ALE-VMS formulation for turbulent flows on moving domains to study the flutter stability limit long-span bridges via the forced-vibration method. We considered a 1:50 scale model of the Hardanger bridge deck, which is a representative for many modern long-span bridge sections.

In order to verify the simulations, corresponding forced-vibration wind tunnel experiments were performed. Comparisons of the aerodynamic derivatives proved the computational framework to capture the self-excited aerodynamic forces with very good accuracy.

Further, the validness of the computations was studied by comparing the predicted responses to free-vibration wind tunnel experiments. The results showed that the forced-vibration method generally predicts the flutter characteristics with good accuracy, and in terms of the mode shape and critical wind speed, the numerical simulations produced equally good estimates as the forced-vibration experiments. The latter was a rather unexpected result, since the two experiments were carefully tuned to match each other. This emphasizes some of the challenges with experimental work, and also that load modeling on bluff-bodies is not an exact science.

The present work have shown, and added some confidence to, that IGA in combination with the ALE-VMS formulation for turbulent flows and the forced-vibration method, can be a powerful tool in the study of flutter on long-span bridges.

8 ACKNOWLEDGMENTS

This work was carried out with financial support from the Norwegian Public Roads Administration. All simulations were performed on resources provided by UNINETT Sigma2 - the National Infrastructure for High Performance Computing and Data Storage in Norway. The authors greatly acknowledge this support.

9 CONCLUSIONS

References

[1] Akkerman, I., Bazilevs, Y., Benson, D.J., Farthing, M.W. and Kees, C.E. Free-Surface Flow and Fluid-Object Interaction Modeling With Emphasis on Ship Hydrodynamics. *J. Appl. Mech.* (2012) **79**:010905.

[2] Akkerman, I., Bazilevs, Y., Kees, C.E. and Farthing, M.W. Isogeometric analysis of free-surface flow. *J. Comput. Phys.* (2011) **230**:4137–4152.

[3] Bazilevs, Y. and Akkerman, I. Large eddy simulation of turbulent Taylor-Couette flow using isogeometric analysis and the residual-based variational multiscale method. *J. Comput. Phys.* (2010) **229**:3402–3414.

[4] Bazilevs, Y., Calo, V., Cottrell, J., Hughes, T., Reali, A. and Scovazzi, G. Variational multiscale residual-based turbulence modeling for large eddy simulation of incompressible flows. *Comput. Methods Appl. Mech. Eng.* (2007) **197**:173–201.

[5] Bazilevs, Y., Calo, V.M., Hughes, T.J.R. and Zhang, Y. Isogeometric fluid-structure interaction: Theory, algorithms, and computations. *Comput. Mech.* (2008) **43**:3–37.

[6] Bazilevs, Y. and Hughes, T.J.R. Weak imposition of Dirichlet boundary conditions in fluid mechanics. *Comput. Fluids* (2007) **36**:12–26.

[7] Bazilevs, Y., Michler, C., Calo, V.M. and Hughes, T.J.R. Weak Dirichlet boundary conditions for wall-bounded turbulent flows. *Comput. Methods Appl. Mech. Eng.* (2007) **196**:4853–4862.

[8] Bazilevs, Y., Michler, C., Calo, V.M. and Hughes, T.J.R. Isogeometric variational multiscale modeling of wall-bounded turbulent flows with weakly enforced boundary conditions on unstretched meshes. *Comput. Methods Appl. Mech. Eng.* (2010) **199**:780–790.

[9] Bazilevs, Y., Takizawa, K. and Tezduyar, T.E. *Computational Fluid-Structure Interaction*. John Wiley & Sons, Ltd, Chichester, UK (2013).

[10] Brooks, A.N. and Hughes, T.J.R. Streamline upwind/Petrov-Galerkin formulations for convection dominated flows with particular emphasis on the incompressible Navier-Stokes equations. *Comput. Methods Appl. Mech. Eng.* (1982) **32**:199–259.

[11] Chen, X. and Kareem, A. Advances in Modeling of Aerodynamic Forces on Bridge Decks. *J. Eng. Mech.* (2002) **128**:1193–1205.

[12] Chung, J. and Hulbert, G.M. A Time Integration Algorithm for Structural Dynamics With Improved Numerical Dissipation: The Generalized-α Method. *J. Appl. Mech.* (1993) **60**:371–375.

[13] Cottrell, J., Reali, A., Bazilevs, Y. and Hughes, T. Isogeometric analysis of structural vibrations. *Comput. Methods Appl. Mech. Eng.* (2006) **195**:5257–5296.

[14] Diana, G., Rocchi, D. and Belloli, M. Wind tunnel : a fundamental tool for long-span bridge design. *Struct. Infrastruct. Eng. Maintenance, Manag. Life-Cycle Des. Perform.* (2015) **11:4**:533–555.

[15] Helgedagsrud, T.A., Bazilevs, Y., Korobenko, A., Mathisen, K.M. and Øiseth, O. Using 3D simulation of turbulent flows on moving domains to compute aerodynamic derivatives of bridge sections. *Comput. Fluids* (2018) .

[16] Helgedagsrud, T.A., Mathisen, K.M., Bazilevs, Y., Øiseth, O. and Korobenko, A. Using ALE-VMS to compute wind forces on moving bridge decks. In B. Skallerud and H.I. Andersson, eds., *Proc. MekIT'17 Ninth Natl. Conf. Comput. Mech.* CMIME, Barcelona, Spain, pp. 169–189.

[17] Hsu, M.C., Akkerman, I. and Bazilevs, Y. High-performance computing of wind turbine aerodynamics using isogeometric analysis. *Comput. Fluids* (2011) **49**:93–100.

[18] Hsu, M.C., Akkerman, I. and Bazilevs, Y. Wind turbine aerodynamics using ALE–VMS: validation and the role of weakly enforced boundary conditions. *Comput. Mech.* (2012) **50**:499–511.

[19] Hsu, M.C., Kamensky, D., Bazilevs, Y., Sacks, M.S. and Hughes, T.J.R. Fluid–structure interaction analysis of bioprosthetic heart valves: significance of arterial wall deformation. *Comput. Mech.* (2014) **54**:1055–1071.

[20] Hughes, T. and Tezduyar, T. Finite element methods for first-order hyperbolic systems with particular emphasis on the compressible euler equations. *Comput. Methods Appl. Mech. Eng.* (1984) **45**:217–284.

[21] Hughes, T.J., Cottrell, J.A. and Bazilevs, Y. Isogeometric analysis: CAD, finite elements, NURBS, exact geometry and mesh refinement. *Comput. Methods Appl. Mech. Eng.* (2005) **194**:4135–4195.

[22] Hughes, T.J., Franca, L.P. and Balestra, M. A new finite element formulation for computational fluid dynamics: V. Circumventing the babuška-brezzi condition: a stable Petrov-Galerkin formulation of the stokes problem accommodating equal-order interpolations. *Comput. Methods Appl. Mech. Eng.* (1986) **59**:85–99.

[23] Hughes, T.J.R. Multiscale phenomena: Green's functions, the Dirichlet-to-Neumann formulation, subgrid scale models, bubbles and the origins of stabilized methods. *Comput. Methods Appl. Mech. Eng.* (1995) **127**:387–401.

[24] Hughes, T.J.R., Feijóo, G.R., Mazzei, L. and Quincy, J.B. The variational multiscale method—a paradigm for computational mechanics. *Comput. Methods Appl. Mech. Eng.* (1998) **166**:3–24.

[25] Hughes, T.J.R., Liu, W.K. and Zimmermann, T.K. Lagrangian-Eulerian finite element formulation for incompressible viscous flows. *Comput. Methods Appl. Mech. Eng.* (1981) **29**:329–349.

[26] Hughes, T.J.R., Mazzei, L. and Jansen, K.E. Large Eddy Simulation and the variational multiscale method. *Comput. Vis. Sci.* (2000) **3**:47–59.

[27] Jansen, K.E., Whiting, C.H. and Hulbert, G.M. A generalized-α method for integrating the filtered Navier-Stokes equations with a stabilized finite element method. *Comput. Methods Appl. Mech. Engrg.* (2000) **190**:305–319.

[28] Johnson, A. and Tezduyar, T. Mesh update strategies in parallel finite element computations of flow problems with moving boundaries and interfaces. *Comput. Methods Appl. Mech. Eng.* (1994) **119**:73–94.

[29] Motlagh, Y.G. and Ahn, H.T. Laminar and turbulent channel flow simulation using residual based variational multi-scale method. *J. Mech. Sci. Technol.* (2012) **26**:447–454.

[30] Øiseth, O., Rönnquist, A. and Sigbjörnsson, R. Simplified prediction of wind-induced response and stability limit of slender long-span suspension bridges, based on modified quasi-steady theory: A case study. *J. Wind Eng. Ind. Aerodyn.* (2010) **98**:730–741.

[31] Øiseth, O. and Sigbjörnsson, R. An alternative analytical approach to prediction of flutter stability limits of cable supported bridges. *J. Sound Vib.* (2011) **330**:2784–2800.

[32] Piegl, L. and Tiller, W. *The NURBS Book*. Monographs in Visual Communications. Springer Berlin Heidelberg, Berlin, Heidelberg (1995).

[33] Scanlan, R.H. and Tomko, J. Airfoil and bridge deck flutter derivatives. *J. Eng. Mech. Div.* (1971) **97**:1717–1737.

[34] Siedziako, B., Øiseth, O. and Rønnquist, A. An enhanced forced vibration rig for wind tunnel testing of bridge deck section models in arbitrary motion. *J. Wind Eng. Ind. Aerodyn.* (2017) **164**:152–163.

[35] Statens Vegvesen. *Håndbok N400 Bruprosjektering* (2015).

[36] Stein, K., Tezduyar, T. and Benney, R. Mesh Moving Techniques for Fluid-Structure Interactions With Large Displacements. *J. Appl. Mech.* (2003) **70**:58.

[37] Svend Ole Hansen APS. The Hardanger bridge: static and dynamic wind tunnel tests with a section model. Technical report, prepared for Norwegian Public Roads Administration. *Technical report* (2006).

[38] Takizawa, K., Bazilevs, Y., Tezduyar, T.E., Hsu, M.C., Øiseth, O., Mathisen, K.M., Kostov, N. and McIntyre, S. Engineering Analysis and Design with ALE-VMS and Space-Time Methods. *Arch. Comput. Methods Eng.* (2014) **21**:481–508.

[39] Takizawa, K., Henicke, B., Puntel, A., Kostov, N. and Tezduyar, T.E. Space-time techniques for computational aerodynamics modeling of flapping wings of an actual locust. *Comput. Mech.* (2012) **50**:743–760.

[40] Takizawa, K., Montes, D., McIntyre, S. and Tezduyar, T.E. Space-time VMS methods for modeling of incompressible flows at high Reynolds numbers. *Math. Model. Methods Appl. Sci.* (2013) **23**:223–248.

[41] Takizawa, K. and Tezduyar, T.E. Multiscale space–time fluid–structure interaction techniques. *Comput. Mech.* (2011) **48**:247–267.

[42] Takizawa, K., Tezduyar, T.E., Mochizuki, H., Hattori, H., Mei, S., Pan, L. and Montel, K. Space–time VMS method for flow computations with slip interfaces (ST-SI). *Math. Model. Methods Appl. Sci.* (2015) **25**:2377–2406.

[43] Takizawa, K., Tezduyar, T.E., Otoguro, Y., Terahara, T., Kuraishi, T. and Hattori, H. Turbocharger flow computations with the Space–Time Isogeometric Analysis (ST-IGA). *Comput. Fluids* (2017) **142**:15–20.

[44] Tezduyar, T., Aliabadi, S., Behr, M., Johnson, A. and Mittal, S. Parallel finite-element computation of 3D flows. *Computer (Long. Beach. Calif).* (1993) **26**:27–36.

[45] Tezduyar, T.E. Computation of moving boundaries and interfaces and stabilization parameters. *Int. J. Numer. Methods Fluids* (2003) **43**:555–575.

[46] Tezduyar, T.E., Behr, M. and Liou, J. A new strategy for finite element computations involving moving boundaries and interfaces – the deforming-spatial-domain/space–time procedure: {I}.˜{T}he concept and the preliminary numerical tests. *Comput. Methods Appl. Mech. Eng.* (1992) **94**:339–351.

[47] Tezduyar, T.E. and Osawa, Y. Finite element stabilization parameters computed from element matrices and vectors. *Comput. Methods Appl. Mech. Eng.* (2000) **190**:411–430.

[48] Tezduyar, T.E. and Park, Y.J. Discontinuity-capturing finite element formulations for nonlinear convection-diffusion-reaction equations. *Comput. Methods Appl. Mech. Eng.* (1986) **59**:307–325.